Y. Wang, F. Topputo, X. Hou
Analytic Gradients in Normalized Low-Thrust Trajectory Optimization with Interior-Point Constraints
Journal of Guidance Control and Dynamics, published online 08/06/2024
doi:10.2514/1.g007896

Analytic Gradients in Normalized Low-Thrust Trajectory Optimization with Interior-Point Constraints

Yang Wang*
Nanjing University, 210023 Nanjing, China

Francesco Topputo†
Polytechnic University of Milan, 20156 Milan, Italy

Xiyun Hou‡
Nanjing University, 210023 Nanjing, China

I. Introduction

Electric propulsion has become a viable option for interplanetary missions [1]. The gravity assist rotates the direction and alters the magnitude of the spacecraft's heliocentric speed vector when passing near the planet [2]. The combination of electric propulsion and gravity-assist technique reduces the overall fuel expenditure [3]. In addition, low-thrust trajectories can be used to flyby (encounter asteroids with the same position, but different velocity) or to rendezvous (encounter asteroids with both the same position and velocity) asteroids to provide useful scientific return [4]. Yet, optimizing low-thrust trajectories with flybys, rendezvous, and gravity assists is a difficult task, due to the extreme sensitivity to the initial guess and the large extent of the search space. It is therefore desirable to elaborate efficient techniques to solve these demanding problems.

With a given sequence of bodies to visit, the low-thrust trajectory optimization with flybys, rendezvous, and gravity assists is a nonlinear optimal control problem (NOCP) with time-dependent, multi-dimensional interior-point constraints. Direct or indirect methods are commonly used to solve the NOCP. Direct methods discretize the NOCP into a nonlinear programming problem, and a solution fulfilling the Karush-Kuhn-Tucker conditions is then searched [5]. Indirect methods solve the NOCP by transforming it into a multi-point boundary value problem (MPBVP) that results from the Pontryagin Minimum Principle (PMP) [5]. Although several advanced tools have been developed in literature using direct methods [3, 6–8], indirect methods provide accurate solutions that satisfy first-order necessary conditions of optimality, yet the initial guess of costates is often nonintuitive [5]. In [9], a normalized low-thrust optimization problem with one gravity assist was formulated by embedding a positive unknown factor into the performance index, which eases the search of unknown costates and multipliers by restricting them on a unit hypersphere. Indirect methods are the focus of this work, and they are becoming increasingly practical with the development of methods such as adjoint scaling

*Postdoctoral Researcher, School of Astronomy and Space Science, Xianlin Avenue 163. E-mail address: yang.wang@nju.edu.cn. (Corresponding author).

†Full Professor, Department of Aerospace Science and Technology, Via La Masa 34. E-mail address: francesco.topputo@polimi.it. AIAA Senior Member.

‡Full Professor, School of Astronomy and Space Science, Xianlin Avenue 163. E-mail address: houxiyun@nju.edu.cn.

technique [10], optimality-preserving transformation [11], and the composite smooth control method [12].

The numerical performance of most optimization methods is highly dependent on the accuracy of the gradient information. Finite difference (FD) methods [13] are easy to implement, yet they are inapproximate for low-thrust trajectory optimization with flybys, rendezvous, and gravity assists because 1) the accuracy of FD methods depends on the step size, which is difficult to tune [14] (Discontinuities produced by interior-point constraints and the bang-bang control further complicate the step selection); 2) The dimension of the search space increases rapidly as more interior-point constraints are involved, and so does the computational burden of FD methods. Analytic gradients obtain gradients by applying the state transition matrix (STM) and the chain rule [15]. Unlike FD methods, analytic gradients do not need a FD step [16]. The benefits of analytic gradients on direct methods with Sims-Flanagan transcription were explored in [8] through a comet sample return mission. For indirect methods, analytic gradients for asteroid rendezvous missions were studied in [4], where both state and costate at each interior-point time were treated as unknowns. The Jacobian matrix of this formulation is sparse and simplified, provided that one has to solve for more unknowns. In [17, 18], the optimal low-thrust gravity-assist trajectory was solved with analytic gradients, which is developed in this work with a more comprehensive analysis on the recursive computation and the derivatives with respect to the interior-point time.

In this Note, analytic gradients are presented for normalized low-thrust trajectory optimization with interior-point constraints. Specifically, the time domain is partitioned into multiple phases with interior-point, initial, and terminal time as boundaries. The integration flowchart in [19] that involves switching detection is applied to the integration within one phase. The chain rule is developed to extend derivatives of constraints from one phase to the whole time domain. The contributions are mainly two-fold: 1) analytic gradients for the normalized low-thrust trajectory optimization problem are derived, including the derivatives with respect to the normalizing factor; 2) recursive formulae to calculate analytic gradients, especially the derivatives with respect to the interior-point time, are developed. The method to generate the initial guess for the energy-optimal problem is not discussed since it is outside the scope of this work. Readers can refer to [9, 20] about generating initial guesses that employ the normalization. The computational framework established in this work combines energy-to-fuel-optimal continuation, switching detection, and analytic gradients, so enabling fuel-optimal bang-bang solutions and their accurate gradients. Two numerical examples are simulated to show the benefits of analytic gradients.

The remainder of the paper is structured as follows. Sec. II introduces the problem statement of low-thrust trajectory optimization with flybys, rendezvous, and gravity assists. Sec. III derives the analytic gradients. Sec. IV presents numerical simulations. Final remarks are given in Conclusions.

II. Problem Statement

A. Fuel-Optimal Problem

The heliocentric phase of an interplanetary transfer subject to the gravitational attraction of the Sun is considered. The equations of motion for the spacecraft are

$$\dot{\boldsymbol{x}} = \boldsymbol{f}(\boldsymbol{x}, u, \boldsymbol{\alpha}) \Rightarrow \begin{cases} \dot{\boldsymbol{r}} = \boldsymbol{v} \\ \dot{\boldsymbol{v}} = -\dfrac{\mu}{r^3}\boldsymbol{r} + u\dfrac{T_{\max}}{m}\boldsymbol{\alpha} \\ \dot{m} = -u\dfrac{T_{\max}}{I_{\text{sp}}\, g_0} \end{cases} \tag{1}$$

where $\boldsymbol{r}$, $\boldsymbol{v}$, and m are the position vector, the velocity vector, and the mass of the spacecraft; $\boldsymbol{x} \coloneqq [\boldsymbol{r}, \boldsymbol{v}, m]$ is the state vector, $u \in [0, 1]$ is the thrust throttle factor, $\boldsymbol{\alpha}$ is the thrust pointing unit vector, $T_{\max}$ is the maximum thrust magnitude, I_{sp} is the specific impulse, and g_0 is the gravitational acceleration at sea level. Both $T_{\max}$ and I_{sp} are assumed constant. With the initial time t_0 and the terminal time t_f given, the fuel-optimal problem is to minimize

$$J_f = \lambda_0 \frac{T_{\max}}{c} \int_{t_0}^{t_f} u \, \mathrm{d}t \tag{2}$$

with boundary conditions

$$\boldsymbol{r}(t_0) - \boldsymbol{r}_0 = 0, \quad \boldsymbol{v}(t_0) - \boldsymbol{v}_0 = 0, \quad m(t_0) - m_0 = 0 \tag{3}$$

$$\boldsymbol{r}(t_f) - \boldsymbol{r}_{\text{T}}(t_f) = 0, \quad \boldsymbol{v}(t_f) - \boldsymbol{v}_{\text{T}}(t_f) = 0 \tag{4}$$

where $\boldsymbol{r}_{\text{T}}(t_f)$ and $\boldsymbol{v}_{\text{T}}(t_f)$ are the position and velocity vectors of the final target body at t_f, respectively, and $c = I_{\text{sp}}\, g_0$. The positive factor λ_0 does not inherently change the NOCP [9] (See Remark 3 for more explanations).

Since the optimal thrust throttle u^* is a discontinuous bang-bang control, the convergence radius is small for zero-finding methods such as Newton's method [21]. Thus, the energy-to-fuel-optimal continuation that approaches the discontinuous control by a series of continuous controls is employed with the performance index as [21]

$$J_\varepsilon = \lambda_0 \frac{T_{\max}}{c} \int_{t_0}^{t_f} [u - \varepsilon u(1 - u)] \, \mathrm{d}t \tag{5}$$

where ε is the embedded continuation parameter. The fuel-optimal problem ($\varepsilon = 0$) is reached by gradually reducing ε from the energy-optimal problem ($\varepsilon = 1$).

The Hamiltonian function of the energy-to-fuel-optimal problem is

$$H_\varepsilon = \boldsymbol{\lambda}_r \cdot \boldsymbol{v} + \boldsymbol{\lambda}_v \cdot \left(-\frac{\mu}{r^3}\boldsymbol{r} + u\frac{T_{\max}}{m}\boldsymbol{\alpha} \right) + \lambda_m \left(-u\frac{T_{\max}}{c} \right) + \lambda_0 \frac{T_{\max}}{c} \left[u - \varepsilon u (1-u) \right] \tag{6}$$

where $\boldsymbol{\lambda} := [\boldsymbol{\lambda}_r, \boldsymbol{\lambda}_v, \lambda_m]$ is the costate vector associated to $\boldsymbol{x}$. According to PMP [22], the optimal thrust pointing unit vector $\boldsymbol{\alpha}^*$ satisfies

$$\boldsymbol{\alpha}^* = -\frac{\boldsymbol{\lambda}_v}{\lambda_v} \tag{7}$$

Substituting Eq. (7) into Eq. (6) yields

$$H_\varepsilon = \boldsymbol{\lambda}_r \cdot \boldsymbol{v} - \frac{\mu}{r^3}\boldsymbol{r} \cdot \boldsymbol{\lambda}_v + \lambda_0 \frac{T_{\max}}{c}\, u \left(S - \varepsilon + \varepsilon u \right) \tag{8}$$

where the throttle switching function S is

$$S = 1 - \frac{\lambda_m}{\lambda_0} - \frac{c}{m\,\lambda_0}\lambda_v \tag{9}$$

The u^* is stated in terms of S and ε as

$$u^* = \begin{cases} 0 & S > \varepsilon \\ 1 & S < -\varepsilon \\ \dfrac{\varepsilon - S}{2\varepsilon} & |S| \leqslant \varepsilon \end{cases} \tag{10}$$

Remark 1 *It is assumed that singular arcs where $S = 0$ in the fuel-optimal problem ($\varepsilon = 0$) are absent over finite time intervals.*

The equations of costate dynamics are

$$\dot{\boldsymbol{\lambda}} = -\left(\frac{\partial H_\varepsilon(\boldsymbol{x}, \boldsymbol{\lambda}, u, \alpha)}{\partial \boldsymbol{x}} \right)^\top \tag{11}$$

Since the terminal mass is free and the augmented terminal cost does not explicitly depend on the mass, the transversality condition for the free terminal mass is

$$\lambda_m(t_f) = 0 \tag{12}$$

The motion of the spacecraft is determined by integrating the following state-costate dynamics

$$\dot{\boldsymbol{y}} = \boldsymbol{F}(\boldsymbol{y}) \Rightarrow \begin{pmatrix} \dot{\boldsymbol{r}} \\ \dot{\boldsymbol{v}} \\ \dot{m} \\ \dot{\boldsymbol{\lambda}}_r \\ \dot{\boldsymbol{\lambda}}_v \\ \dot{\lambda}_m \end{pmatrix} = \begin{pmatrix} \boldsymbol{v} \\ -\dfrac{\mu}{r^3}\boldsymbol{r} - u^* \dfrac{T_{\max}}{m} \dfrac{\boldsymbol{\lambda}_v}{\lambda_v} \\ -u^* \dfrac{T_{\max}}{c} \\ -\dfrac{3\mu}{r^5}(\boldsymbol{r} \cdot \boldsymbol{\lambda}_v)\,\boldsymbol{r} + \dfrac{\mu}{r^3}\boldsymbol{\lambda}_v \\ -\boldsymbol{\lambda}_r \\ -\dfrac{u^* \lambda_v T_{\max}}{m^2} \end{pmatrix} \tag{13}$$

where $\boldsymbol{y} := [\boldsymbol{x}, \boldsymbol{\lambda}] \in \mathbb{R}^{14}$, and $\boldsymbol{\alpha}^*$ in Eq. (7) and u^* in Eq. (10) are already embedded into Eq. (13).

B. Interior-Point Constraints

Let $\boldsymbol{x}$ be partitioned as $\boldsymbol{x} = [\boldsymbol{x}_c, \boldsymbol{x}_d, \tilde{\boldsymbol{x}}]$ where $\boldsymbol{x}_c$ and $\boldsymbol{x}_d$ are the continuous and the discontinuous state component involved in the interior-point constraints at the interior-point time t_j, $j = 1, 2, \cdots, w$, respectively, $\tilde{\boldsymbol{x}}$ is the remaining part of the state, and w is the total number of the interior-point time. The bold vector notation $\tilde{\boldsymbol{x}}$ is used even though it may be a scalar variable in specific applications. The equality interior-point constraints at t_j are denoted as

$$\boldsymbol{h}_j(t_j, \boldsymbol{x}_c(t_j)) = \boldsymbol{0}, \quad \boldsymbol{h}_j \in \mathbb{R}^{p_j} \tag{14}$$

$$\phi_j(t_j, \boldsymbol{x}_d(t_j^-), \boldsymbol{x}_d(t_j^+)) = 0 \tag{15}$$

The inequality interior-point constraint at t_j is denoted as

$$\sigma_j(t_j, \boldsymbol{x}_d(t_j^-), \boldsymbol{x}_d(t_j^+)) \leqslant 0 \tag{16}$$

where ϕ_j in Eq. (15) and σ_j in Eq. (16) are scalar constraints. Let $\boldsymbol{\lambda}_c$, $\boldsymbol{\lambda}_d$ and $\tilde{\boldsymbol{\lambda}}$ be the costate vectors associated to $\boldsymbol{x}_c$, $\boldsymbol{x}_d$ and $\tilde{\boldsymbol{x}}$, respectively. Here below we specialize Eqs. (14)-(16) for two categories:

1. Interplanetary transfer with flybys and rendezvous

1) Intermediate flyby. In this case, $\boldsymbol{x}_c := \boldsymbol{r}$, $\tilde{\boldsymbol{x}} := [\boldsymbol{v}, m]$, $\boldsymbol{\lambda}_c := \boldsymbol{\lambda}_r$, $\tilde{\boldsymbol{\lambda}} := [\boldsymbol{\lambda}_v, \lambda_m]$, then

$$\boldsymbol{h}_j(t_j, \boldsymbol{x}_c(t_j)) = \boldsymbol{r}(t_j) - \boldsymbol{r}_{\mathrm{T},j}(t_j), \quad p_j = 3 \tag{17}$$

where $\boldsymbol{r}_{\mathrm{T},j}(t_j)$ is the position vector of jth body in the sequence at t_j.

2) Intermediate rendezvous. In this case, $\boldsymbol{x}_c \coloneqq [\boldsymbol{r}, \boldsymbol{v}]$, $\tilde{\boldsymbol{x}} \coloneqq m$, $\boldsymbol{\lambda}_c \coloneqq [\boldsymbol{\lambda}_r, \boldsymbol{\lambda}_v]$, $\tilde{\boldsymbol{\lambda}} \coloneqq \lambda_m$, then

$$\boldsymbol{h}_j(t_j, \boldsymbol{x}_c(t_j)) = [\boldsymbol{r}(t_j) - \boldsymbol{r}_{\mathrm{T},j}(t_j), \quad \boldsymbol{v}(t_j) - \boldsymbol{v}_{\mathrm{T},j}(t_j)], \quad p_j = 6 \tag{18}$$

where $\boldsymbol{v}_{\mathrm{T},j}(t_j)$ is the velocity vector of jth body in the sequence at t_j.

In this category, there are no constraints expressed by ϕ_j and σ_j. The necessary conditions of optimality for interior-point constraints at t_j are [22]

$$\chi_j^\top \frac{\partial \boldsymbol{h}_j}{\partial t_j} + H_\varepsilon(\boldsymbol{y}(t_j^-), \lambda_0) - H_\varepsilon(\boldsymbol{y}(t_j^+), \lambda_0) = 0 \tag{19}$$

$$\chi_j^\top \frac{\partial \boldsymbol{h}_j}{\partial \boldsymbol{x}_c} - \boldsymbol{\lambda}_c^\top(t_j^-) + \boldsymbol{\lambda}_c^\top(t_j^+) = \boldsymbol{0}^\top \tag{20}$$

where $\chi_j \in \mathbb{R}^{p_j}$ is the multiplier vector associated to the constraint $\boldsymbol{h}_j$.

2. Interplanetary transfer with gravity assists The unpowered gravity-assist transfer [9] is considered. Let r_p be the radius of gravity-assist maneuver and $\hat{\boldsymbol{\imath}}(t_j^\pm) \coloneqq \boldsymbol{v}_\infty^\pm / v_\infty^\pm$ where $v_\infty^\pm = \|\boldsymbol{v}_\infty^\pm\|$ and $\boldsymbol{v}_\infty^\pm = \boldsymbol{v}(t_j^\pm) - \boldsymbol{v}_{\mathrm{T},j}(t_j)$, then r_p is computed as [9]

$$\cos\theta = \hat{\boldsymbol{\imath}}(t_j^-) \cdot \hat{\boldsymbol{\imath}}(t_j^+) \tag{21}$$

$$r_p = \frac{\mu_j}{v_\infty^- v_\infty^+} \left(\frac{1}{\sin(\theta/2) - 1} \right) \tag{22}$$

where θ is the deflection angle and μ_j is the gravity parameter of the gravity-assist planet.

In this case, $\boldsymbol{x}_c \coloneqq \boldsymbol{r}$, $\boldsymbol{x}_d \coloneqq \boldsymbol{v}$, $\tilde{\boldsymbol{x}} \coloneqq m$, $\boldsymbol{\lambda}_c \coloneqq \boldsymbol{\lambda}_r$, $\boldsymbol{\lambda}_d \coloneqq \boldsymbol{\lambda}_v$, $\tilde{\boldsymbol{\lambda}} \coloneqq \lambda_m$, and

$$\boldsymbol{h}_j(t_j, \boldsymbol{x}_c(t_j)) = \boldsymbol{r}(t_j) - \boldsymbol{r}_{\mathrm{T},j}(t_j), \quad p_j = 3 \tag{23}$$

$$\phi_j(t_j, \boldsymbol{x}_d(t_j^-), \boldsymbol{x}_d(t_j^+)) = v_\infty^- - v_\infty^+ \tag{24}$$

$$\sigma_j(t_j, \boldsymbol{x}_d(t_j^-), \boldsymbol{x}_d(t_j^+)) = 1 - r_p/r_{\min} \leqslant 0 \tag{25}$$

where $r_{\min}$ is the minimum radius required to perform the gravity assist.

The slack variable α_j is introduced to transform the inequality constraint Eq. (25) into the equality constraint, as [23]

$$\sigma_j(t_j, \boldsymbol{x}_d(t_j^-), \boldsymbol{x}_d(t_j^+)) + \alpha_j^2 = 0 \tag{26}$$

Suppose that the corresponding multiplier is κ_j, it must satisfy

$$\kappa_j \alpha_j = 0 \tag{27}$$

The method to cope with the inequality constraint of Eq. (25) is different from the work in [9] where conditions $\kappa_j \sigma_j = 0$ and $\kappa_j \geqslant 0$ are applied. The advantage of Eqs. (26) and (27) is that it is unnecessary to judge the sign of κ_j, but the drawback is the addition of one unknown variable α_j. Equations (26) and (27) are used, yet analytic gradients derived in this work can be easily adjusted when $\kappa_j \sigma_j = 0$ is applied.

The necessary conditions of optimality for interior-point constraints at t_j are

$$\boldsymbol{\chi}_j^\top \left[\frac{\partial \boldsymbol{h}_j}{\partial t_j}, \frac{\partial \phi_j}{\partial t_j} \right] + \kappa_j \frac{\partial \sigma_j}{\partial t_j} + H_{\varepsilon,j}(\boldsymbol{y}(t_j^-), \lambda_0) - H_{\varepsilon,j}(\boldsymbol{y}(t_j^+), \lambda_0) = 0 \tag{28}$$

$$\boldsymbol{\chi}_{c,j}^\top \frac{\partial \boldsymbol{h}_j}{\partial \boldsymbol{x}_c} - \boldsymbol{\lambda}_c^\top(t_j^-) + \boldsymbol{\lambda}_c^\top(t_j^+) = \boldsymbol{0}^\top \tag{29}$$

$$\chi_{d,j} \frac{\partial \phi_j}{\partial \boldsymbol{x}_d(t_j^-)} - \boldsymbol{\lambda}_d^\top(t_j^-) + \kappa_j \frac{\partial \sigma_j}{\partial \boldsymbol{x}_d(t_j^-)} = \boldsymbol{0}^\top \tag{30}$$

$$\chi_{d,j} \frac{\partial \phi_j}{\partial \boldsymbol{x}_d(t_j^+)} + \boldsymbol{\lambda}_d^\top(t_j^+) + \kappa_j \frac{\partial \sigma_j}{\partial \boldsymbol{x}_d(t_j^+)} = \boldsymbol{0}^\top \tag{31}$$

where $\boldsymbol{\chi}_j = [\boldsymbol{\chi}_{c,j}^\top, \chi_{d,j}]^\top \in \mathbb{R}^{p_j+1}$ is the multiplier vector associated to Eqs. (23) and (24).

Remark 2 *Let $\boldsymbol{y}(t) = \boldsymbol{\varphi}_\varepsilon(\boldsymbol{y}_i, \lambda_0, t_0, t)$ be the solution flow of Eq.* (13) *from the initial time t_0 to the terminal time t_f, using $\boldsymbol{y}_i$ at t_0, λ_0, $\boldsymbol{\lambda}_c(t_n^+)$ in Eq.* (20) *at flyby or rendezvous time t_n ($n = 1, \cdots, \hat{w}$), $\boldsymbol{\lambda}_c(t_j^+)$ in Eq.* (29) *and $\boldsymbol{\lambda}_d(t_j^+)$ in Eq.* (31) *at gravity-assist time t_j ($j = \hat{w}+1, \cdots, w$), the energy-to-fuel-optimal problem is to find $[\lambda_0, \boldsymbol{\lambda}_i, \boldsymbol{\chi}_n, t_n, \boldsymbol{\chi}_j, \boldsymbol{x}_d(t_j^+), \alpha_j, \kappa_j, t_j]$ such that $\boldsymbol{y}(t)$ satisfies* (4), (12) *at t_f,* (17) *(for flyby),* (18) *(for rendezvous),* (19) *at t_n,* (23), (24), (26), (27), (28), (30) *at t_j, and the normalization condition as*

$$\sqrt{\lambda_0^2 + \boldsymbol{\lambda}_i^\top \boldsymbol{\lambda}_i + \sum_{n=1}^{\hat{w}} \boldsymbol{\chi}_n^\top \boldsymbol{\chi}_n + \sum_{j=\hat{w}+1}^{w} (\boldsymbol{\chi}_j^\top \boldsymbol{\chi}_j + \kappa_j^2)} - 1 = 0 \tag{32}$$

Remark 3 *Since the equations mentioned in Remark 2, as well as the Hamiltonian function Eq.* (8) *and the switching function Eq.* (9)*, that formulate the MPBVP are all homogeneous to λ_0, $\boldsymbol{\lambda}_i$, $\boldsymbol{\chi}_j$, κ_j, and $\boldsymbol{\chi}_n$, multiplying them by a positive factor does not change the problem. The value of λ_0 should be positive, otherwise the problem is changed to maximize the fuel consumption. Let $\boldsymbol{\lambda}_{\text{all}}$ be the collection of multipliers and initial costates, then $\hat{\boldsymbol{\lambda}}_{\text{all}} = \boldsymbol{\lambda}_{\text{all}} / \|\boldsymbol{\lambda}_{\text{all}}\|$ would lead to the same result. Let $\hat{\boldsymbol{\lambda}}_{\text{all}}$ be the desired solution, then the normalization condition in Eq.* (32) *is introduced.*

Remark 4 *The value of λ_0 should be fixed for a given ε, and can be varied as ε varies during the energy-to-fuel-optimal continuation. In [9], the value of λ_0 remains fixed during the continuation. Here, we allow varying λ_0 during the continuation to search the solution in a higher dimension of the search space. In addition, the procedure to calculate derivatives of constraints with respect to λ_0 in Sec. III is general and can be applied to computing derivatives with respect to other parameters, such as $T_{\max}$ or I_{sp}. In this case, our method can provide the information about how* *constraints vary as $T_{\max}$ or I_{sp} varies.*

III. Indirect Method

A. State Transition Matrix

The STM gives the linear relationship of small displacements of state and costate between different time instants along a continuous trajectory [15]. However, a variety of discontinuities exist in the problem. The bang-bang control is produced by Eq. (10) for the fuel-optimal problem. The costate discontinuity in Eqs. (20), (29) and (31) occurs at the interior-point time, and the spacecraft's velocity is discontinues across the gravity-assist time. Thus, the analysis of STM across the discontinuity should be performed, as well as the derivative of $\boldsymbol{y}$ with respect to λ_0. Since discontinuities caused by interior-point constraints only exist at the interior-point time, the time domain is partitioned into multiple phases. With reference to Fig. 1, t_k denotes the generic interior-point time t_j if $k = 1, \cdots, w$, and denotes the initial time t_0 if $k = 0$. The STM is computed by sweeping each phase consecutively, with interior-point time t_j, initial time t_0, and terminal time t_f as boundaries. Within the $(k+1)$th phase, the STM is subject to the variational equation

$$\dot{\Phi}(t, t_k^+) = D_y \boldsymbol{F}\, \Phi(t, t_k^+), \quad k = 0, 1, \cdots, w \tag{33}$$

where $t \in [t_k^+, t_{k+1}^-]$, $t_0^+ := t_0$, $t_{w+1}^- := t_f$, $\Phi(t_k^+, t_k^+) = I_{14\times 14}$, and $D_y \boldsymbol{F} := \partial \boldsymbol{F}/\partial \boldsymbol{y}$ is the Jacobian matrix of Eq. (13). Two different expressions of $D_y \boldsymbol{F}$ exist based on whether u^* is constant or not [19]. For simplicity of notations, a general variable $\boldsymbol{x}(t_k^\pm)$ is simplified as $\boldsymbol{x}_k^\pm$ in the following, unless otherwise specified.

Considering that the value of $\boldsymbol{y}_k^+$ is affected by perturbing λ_0, the full derivative $\boldsymbol{\zeta} = \mathrm{d}\boldsymbol{y}/\mathrm{d}\lambda_0$ is used and $\boldsymbol{\zeta}$ can be expressed as

$$\boldsymbol{\zeta} = \frac{\partial \boldsymbol{y}}{\partial \lambda_0} + \frac{\partial \boldsymbol{y}}{\partial \boldsymbol{y}_k^+} \frac{\mathrm{d}\boldsymbol{y}_k^+}{\mathrm{d}\lambda_0} \tag{34}$$

The time derivative of $\boldsymbol{\zeta}$ satisfies

$$\dot{\boldsymbol{\zeta}} = D_y \boldsymbol{F}\, \boldsymbol{\zeta} + \frac{\partial \boldsymbol{F}}{\partial \lambda_0} \tag{35}$$

where $\partial \boldsymbol{F}/\partial \lambda_0$ is non-zero if $u^* = (\varepsilon - S)/(2\varepsilon)$, and $\boldsymbol{\zeta}(t_0) = \boldsymbol{0}_{14\times 1}$ at t_0.

Let $\boldsymbol{z} = [\boldsymbol{y}, \text{vec}(\Phi), \boldsymbol{\zeta}] \in \mathbb{R}^{224}$ where 'vec' maps Φ to a column vector, then

$$\dot{\boldsymbol{z}} = \boldsymbol{G}(\boldsymbol{z}) \Rightarrow \begin{cases} \dot{\boldsymbol{y}} & = \boldsymbol{F}(\boldsymbol{y}) \\ \text{vec}(\dot{\Phi}) & = \text{vec}(D_y \boldsymbol{F}\, \Phi) \\ \dot{\boldsymbol{\zeta}} & = D_y \boldsymbol{F}\, \boldsymbol{\zeta} + \dfrac{\partial \boldsymbol{F}}{\partial \lambda_0} \end{cases} \tag{36}$$

with $\boldsymbol{z}_k^+ = [\boldsymbol{y}_k^+, \text{vec}(I_{14\times 14}), \boldsymbol{\zeta}_k^+]$ as the initial value to integrate Eq. (36) from t_k^+ to t_{k+1}^-.

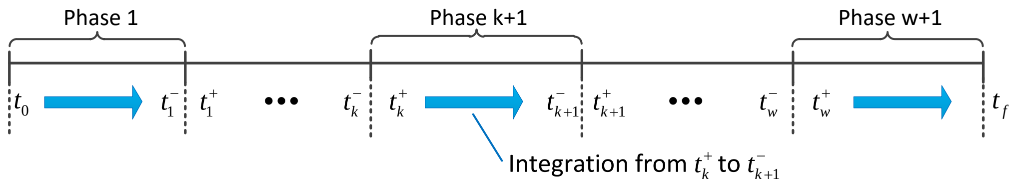

Fig. 1 Integration is performed on each phase consecutively.

At the switching time $t_s \in (t_k^+, t_{k+1}^-)$ where $S(t_s) = \varepsilon$ or $S(t_s) = -\varepsilon$, the STM across t_s is calculated as [24]

$$\Psi(t_s) = \frac{\partial \boldsymbol{y}_s^+}{\partial \boldsymbol{y}_s^-} = I_{14\times 14} + \left(\dot{\boldsymbol{y}}_s^+ - \dot{\boldsymbol{y}}_s^-\right) \frac{1}{\dot{S}} \frac{\partial S}{\partial \boldsymbol{y}} \tag{37}$$

Also, we can obtain

$$\frac{\mathrm{d}\boldsymbol{y}_s^+}{\mathrm{d}\lambda_0} = \frac{\mathrm{d}\boldsymbol{y}_s^-}{\mathrm{d}\lambda_0} + \left(\dot{\boldsymbol{y}}_s^+ - \dot{\boldsymbol{y}}_s^-\right) \frac{1}{\dot{S}} \left(\frac{\partial S}{\partial \boldsymbol{y}} \frac{\mathrm{d}\boldsymbol{y}_s^-}{\mathrm{d}\lambda_0} + \frac{\partial S}{\partial \lambda_0} \right) \tag{38}$$

where $\dot{S} = (c\boldsymbol{\lambda}_r \cdot \boldsymbol{\lambda}_v) / (m\lambda_0\lambda_v)$.

Suppose that the epochs of the switching time are located at $t_{s,1}, t_{s,2}, \cdots, t_{s,N} \in (t_k^+, t_{k+1}^-)$, $\Phi(t_{k+1}^-, t_k^+)$ is calculated using the chain rule as

$$\Phi(t_{k+1}^-, t_k^+) = \Phi(t_{k+1}^-, t_{s,N}^+)\Psi(t_{s,N})\Phi(t_{s,N}^-, t_{s,N-1}^+)\Psi(t_{s,N-1}) \cdots \Phi(t_{s,2}^-, t_{s,1}^+)\Psi(t_{s,1})\Phi(t_{s,1}^-, t_k^+) \tag{39}$$

Then $\Phi(t_f, t_0)$ is computed as

$$\begin{aligned} \Phi(t_f, t_0) &= \Phi(t_f, t_w^+)\frac{\partial \boldsymbol{y}_w^+}{\partial \boldsymbol{y}_w^-}\Phi(t_w^-, t_{w-1}^+) \cdots \frac{\partial \boldsymbol{y}_{k+1}^+}{\partial \boldsymbol{y}_{k+1}^-}\Phi(t_{k+1}^-, t_k^+) \cdots \frac{\partial \boldsymbol{y}_1^+}{\partial \boldsymbol{y}_1^-}\Phi(t_1^-, t_0) \\ &= \Phi(t_f, t_w^+)\Phi(t_w^+, t_{w-1}^+) \cdots \Phi(t_{k+1}^+, t_k^+) \cdots \Phi(t_1^+, t_0) \end{aligned} \tag{40}$$

where $\Phi(t_{k+1}^+, t_k^+) := \partial \boldsymbol{y}_{k+1}^+ / \partial \boldsymbol{y}_k^+ = \partial \boldsymbol{y}_{k+1}^+ / \partial \boldsymbol{y}_{k+1}^- \Phi(t_{k+1}^-, t_k^+)$.

Meanwhile, $\boldsymbol{\zeta}_{k+1}^-$ is obtained by integrating Eq. (35) with $\boldsymbol{\zeta}_s^+$ determined by Eq. (38), and $\boldsymbol{\zeta}_{k+1}^+$ satisfies

$$\boldsymbol{\zeta}_{k+1}^+ = \frac{\partial \boldsymbol{y}_{k+1}^+}{\partial \boldsymbol{y}_{k+1}^-}\boldsymbol{\zeta}_{k+1}^- \tag{41}$$

It can be seen from Eq. (40) that the interior-point time should be provided to accurately calculate $\Phi(t_f, t_0)$. In this work, the interior-point time is provided by the guess solution. In addition, the common integration algorithm with a variable step has the issue of inaccuracy because of the discontinuous right-hand side of Eq. (36) [21]. Thus, it is essential to combine a variable-step integrator with the switching detection. In this aspect, the integration flowchart in [19] that combines the 7/8th-order Runge-Kutta scheme with the switching detection is employed to integrate Eq. (36).

The t_s is located by dichotomy such that $S(t_s) = \varepsilon$ or $S(t_s) = -\varepsilon$ when S crosses ε or $-\varepsilon$ values.

B. Derivatives of State and Costate

The differential of $\boldsymbol{y}_k^+$ at the interior-point time, i.e., $\boldsymbol{y}_j^+$, as well as $\boldsymbol{y}(t_f)$, for two categories of applications are depicted. Derivatives obtained in this section are necessary to specialize $\Phi(t_{k+1}^+, t_k^+)$ in Eq. (40) and $\boldsymbol{\zeta}_{k+1}^+$ in Eq. (41).

1. Interplanetary transfer with flybys and rendezvous The differential of $\boldsymbol{y}_j^+$ is

$$\mathrm{d}\boldsymbol{y}_j^+ = \Phi(t_j^+, t_{j-1}^+)\mathrm{d}\boldsymbol{y}_{j-1}^+ + \frac{\partial \boldsymbol{y}_j^+}{\partial \boldsymbol{\chi}_j}\mathrm{d}\boldsymbol{\chi}_j + \frac{\partial \boldsymbol{y}_j^+}{\partial \lambda_0}\mathrm{d}\lambda_0 + \frac{\mathrm{d}\boldsymbol{y}_j^+}{\mathrm{d}t_j}\mathrm{d}t_j + \sum_{q=1}^{j-1}\frac{\partial \boldsymbol{y}_j^+}{\partial t_q}\mathrm{d}t_q \tag{42}$$

where

$$\Phi(t_j^+, t_{j-1}^+) = \frac{\partial \boldsymbol{y}_j^-}{\partial \boldsymbol{y}_{j-1}^+}, \quad \frac{\partial \boldsymbol{y}_j^+}{\partial \boldsymbol{\chi}_j} = \begin{bmatrix} \boldsymbol{0}_{7\times p_j} \\ -\boldsymbol{h}_{c,j}^\top \\ \boldsymbol{0}_{(7-p_j)\times p_j} \end{bmatrix}, \quad \frac{\partial \boldsymbol{y}_j^+}{\partial \lambda_0} = \frac{\partial \boldsymbol{y}_j^-}{\partial \lambda_0} \tag{43}$$

and

$$\frac{\mathrm{d}\boldsymbol{y}_j^+}{\mathrm{d}t_j} = \hat{\boldsymbol{y}}_{t,j}^+ + \check{\boldsymbol{y}}_{t,j}^+ \tag{44}$$

with $\boldsymbol{h}_{c,j} = \partial \boldsymbol{h}_j/\partial \boldsymbol{x}_c$ being a constant matrix. In this category, since $\partial \boldsymbol{y}_j^+/\partial \boldsymbol{y}_j^- = I_{14\times 14}$, y_j^+ and y_j^- are interchangeable for derivatives such as $\Phi(t_j^+, t_{j-1}^+)$. In Eq. (44), $\hat{\boldsymbol{y}}_{t,j}^+ := \left(\partial \boldsymbol{y}_j^+/\partial \boldsymbol{y}_j^-\right)\dot{\boldsymbol{y}}_j^- = \dot{\boldsymbol{y}}_j^-$ and $\check{\boldsymbol{y}}_{t,j}^+ := \partial \boldsymbol{y}_j^+/\partial t_j = \boldsymbol{0}_{14\times 1}$ are terms that implicitly and explicitly depend on t_j, respectively. The last term in Eq. (42), as well as terms related to $\mathrm{d}t_q$ in the following, will be discussed in Sec. III.C.

The $\boldsymbol{\zeta}_j^+$ satisfies

$$\boldsymbol{\zeta}_j^+ = \boldsymbol{\zeta}_j^- \tag{45}$$

The vectors $\boldsymbol{y}_j^+ = [\boldsymbol{x}_j^-, \boldsymbol{\lambda}_{c,j}^- - \boldsymbol{h}_{c,j}^\top \boldsymbol{\chi}_j, \tilde{\boldsymbol{\lambda}}_j^-]$ and $\boldsymbol{\zeta}_j^+$ in Eq. (45) are used to integrate Eq. (36) within $[t_j^+, t_{j+1}^-]$.

2. Interplanetary transfer with gravity assists The differential of $\boldsymbol{y}_j^+$ is

$$\mathrm{d}\boldsymbol{y}_j^+ = \Phi(t_j^+, t_{j-1}^+)\mathrm{d}\boldsymbol{y}_{j-1}^+ + \frac{\partial \boldsymbol{y}_j^+}{\partial \boldsymbol{x}_{d,j}^+}\mathrm{d}\boldsymbol{x}_{d,j}^+ + \frac{\partial \boldsymbol{y}_j^+}{\partial \boldsymbol{\chi}_j}\mathrm{d}\boldsymbol{\chi}_j + \frac{\partial \boldsymbol{y}_j^+}{\partial \kappa_j}\mathrm{d}\kappa_j + \frac{\mathrm{d}\boldsymbol{y}_j^+}{\mathrm{d}t_j}\mathrm{d}t_j + \frac{\partial \boldsymbol{y}_j^+}{\partial \lambda_0}\mathrm{d}\lambda_0 + \sum_{q=1}^{j-1}\frac{\partial \boldsymbol{y}_j^+}{\partial t_q}\mathrm{d}t_q \tag{46}$$

where

$$
\Phi(t_j^+, t_{j-1}^+) = \begin{bmatrix} \dfrac{\partial \boldsymbol{x}_{c,j}^-}{\partial \boldsymbol{y}_{k-1}^+} \\ \boldsymbol{0}_{3\times 14} \\ \dfrac{\partial \tilde{\boldsymbol{x}}_j^-}{\partial \boldsymbol{y}_{j-1}^+} \\ \dfrac{\partial \boldsymbol{\lambda}_{c,j}^-}{\partial \boldsymbol{y}_{j-1}^+} \\ \dfrac{\partial \boldsymbol{\lambda}_{d,j}^+}{\partial \boldsymbol{y}_{j-1}^+} \\ \dfrac{\partial \tilde{\boldsymbol{\lambda}}_j^-}{\partial \boldsymbol{y}_{j-1}^+} \end{bmatrix}, \quad \frac{\partial \boldsymbol{y}_j^+}{\partial \boldsymbol{x}_{d,j}^+} = \begin{bmatrix} \boldsymbol{0}_{3\times 3} \\ \boldsymbol{I}_{3\times 3} \\ \boldsymbol{0}_{4\times 3} \\ \dfrac{\partial \boldsymbol{\lambda}_{d,j}^+}{\partial \boldsymbol{x}_{d,j}^+} \\ \boldsymbol{0}_{1\times 3} \end{bmatrix}, \quad \frac{\partial \boldsymbol{y}_j^+}{\partial \boldsymbol{\chi}_j} = \begin{bmatrix} \boldsymbol{0}_{7\times 4} \\ \dfrac{\partial \boldsymbol{\lambda}_{c,j}^+}{\partial \boldsymbol{\chi}_j} \\ \dfrac{\partial \boldsymbol{\lambda}_{d,j}^+}{\partial \boldsymbol{\chi}_j} \\ \boldsymbol{0}_{1\times 4} \end{bmatrix}, \quad \frac{\partial \boldsymbol{y}_j^+}{\partial \kappa_j} = \begin{bmatrix} \boldsymbol{0}_{10\times 1} \\ \dfrac{\partial \boldsymbol{\lambda}_{d,j}^+}{\partial \kappa_j} \\ 0 \end{bmatrix}, \quad \frac{\partial \boldsymbol{y}_j^+}{\partial \lambda_0} = \begin{bmatrix} \dfrac{\partial \boldsymbol{x}_{c,j}^-}{\partial \lambda_0} \\ \boldsymbol{0}_{3\times 1} \\ \dfrac{\partial \tilde{\boldsymbol{x}}_j^-}{\partial \lambda_0} \\ \dfrac{\partial \boldsymbol{\lambda}_{c,j}^-}{\partial \lambda_0} \\ \dfrac{\partial \boldsymbol{\lambda}_{d,j}^+}{\partial \lambda_0} \\ \dfrac{\partial \tilde{\boldsymbol{\lambda}}_j^-}{\partial \lambda_0} \end{bmatrix} \tag{47}
$$

and

$$
\frac{\mathrm{d}\boldsymbol{y}_j^+}{\mathrm{d}t_j} = \widehat{\boldsymbol{y}}_{t,j}^+ + \check{\boldsymbol{y}}_{t,j}^+ \tag{48}
$$

with

$$
\widehat{\boldsymbol{y}}_{t,j}^+ = \begin{bmatrix} \dot{\boldsymbol{x}}_{c,j}^- \\ \boldsymbol{0}_{3\times 1} \\ \dot{\tilde{\boldsymbol{x}}}_j^- \\ \dot{\boldsymbol{\lambda}}_{c,j}^- \\ -\dfrac{\partial \boldsymbol{\sigma}_{d,j+}^\top \kappa_j}{\partial \boldsymbol{x}_{d,j}^-} \dot{\boldsymbol{x}}_{d,j}^- \\ \dot{\tilde{\boldsymbol{\lambda}}}_j^- \end{bmatrix} \quad \check{\boldsymbol{y}}_{t,j}^+ = \begin{bmatrix} \boldsymbol{0}_{10\times 1} \\ -\left(\dfrac{\partial \boldsymbol{\phi}_{d,j+}^\top \chi_{d,j}}{\partial t_j} + \dfrac{\partial \boldsymbol{\sigma}_{d,j+}^\top \kappa_j}{\partial t_j} \right) \\ 0 \end{bmatrix} \tag{49}
$$

Here, $\check{\boldsymbol{y}}_{t,j}^+$ is a non-zero vector.

The $\boldsymbol{\zeta}_j^+$ satisfies

$$
\boldsymbol{\zeta}_j^+ = \begin{bmatrix} \boldsymbol{I}_{3\times 3} & & & & & \\ & \boldsymbol{0}_{3\times 3} & & & & \\ & & 1 & & & \\ & & & \boldsymbol{I}_{3\times 3} & & \\ & -\dfrac{\partial \boldsymbol{\sigma}_{d,j+}^\top \kappa}{\partial \boldsymbol{x}_{d,j}^-} & & & & \\ & & & & & 1 \end{bmatrix} \boldsymbol{\zeta}_j^- \tag{50}
$$

where $\boldsymbol{\sigma}_{d,j+}(t, \boldsymbol{x}_{d,j}^-, \boldsymbol{x}_{d,j}^+) = \partial \sigma_j / \partial \boldsymbol{x}_{d,j}^+$ and $\boldsymbol{\phi}_{d,j+}(t, \boldsymbol{x}_{d,j}^+) = \partial \phi_j / \partial \boldsymbol{x}_{d,j}^+$. The vector $\boldsymbol{y}_j^+ = [\boldsymbol{x}_{c,j}^-, \boldsymbol{x}_{d,j}^+, \tilde{\boldsymbol{x}}_j^-, \boldsymbol{\lambda}_{c,j}^- - \boldsymbol{h}_{c,j}^\top \boldsymbol{\chi}_{c,j}, -\boldsymbol{\phi}_{d,j+}^\top \chi_{d,j} - \boldsymbol{\sigma}_{d,j+}^\top \kappa_j, \tilde{\boldsymbol{\lambda}}_j^-]$ and $\boldsymbol{\zeta}_k^+$ in Eq. (50) are used to integrate Eq. (36) within $[t_j^+, t_{j+1}^-]$.

The differential of $\boldsymbol{y}(t_f)$ is the same for both categories, as

$$\mathrm{d}\boldsymbol{y}(t_f) = \frac{\partial \boldsymbol{y}(t_f)}{\partial \boldsymbol{y}_w^+}\mathrm{d}\boldsymbol{y}_w^+ + \frac{\partial \boldsymbol{y}(t_f)}{\partial \lambda_0}\mathrm{d}\lambda_0 + \sum_{q=1}^{w} \frac{\partial \boldsymbol{y}(t_f)}{\partial t_q}\mathrm{d}t_q \tag{51}$$

where the term related to $\mathrm{d}t_f$ does not exist, since t_f is fixed.

C. Derivatives of Constraints and the Chain Rule

Once derivatives in Sec. III.A and Sec. III.B are obtained, gradients of constraints at t_j can be computed via two steps: the derivation of constraints with respect to decision variables at t_j, and the application of the chain rule to calculate derivatives of constraints with respect to decision variables at t_{j-q}, $q \geqslant 1$. For the first step, the differential of a general constraint $\mathcal{N}_j(t_j, \lambda_0, \boldsymbol{y}_j^-, \boldsymbol{y}_j^+, \boldsymbol{\chi}_j, \boldsymbol{\kappa}_j, \alpha_j)$ is

$$\begin{aligned}\mathrm{d}\mathcal{N}_j = {} & \frac{\partial \mathcal{N}_j}{\partial \boldsymbol{y}_{j-1}^+}\mathrm{d}\boldsymbol{y}_{j-1}^+ + \frac{\partial \mathcal{N}_j}{\partial \boldsymbol{x}_{d,j}^+}\mathrm{d}\boldsymbol{x}_{d,j}^+ + \frac{\partial \mathcal{N}_j}{\partial \boldsymbol{\chi}_j}\mathrm{d}\boldsymbol{\chi}_j + \frac{\partial \mathcal{N}_j}{\partial \boldsymbol{\kappa}_j}\mathrm{d}\boldsymbol{\kappa}_j + \frac{\partial \mathcal{N}_j}{\partial \alpha_j}\mathrm{d}\alpha_j + \frac{\mathrm{d}\mathcal{N}_j}{\mathrm{d}t_j}\mathrm{d}t_j \\ & + \left(\frac{\partial \mathcal{N}_j}{\partial \boldsymbol{y}_j^-}\frac{\partial \boldsymbol{y}_j^-}{\partial \lambda_0} + \frac{\partial \mathcal{N}_j}{\partial \boldsymbol{y}_j^+}\frac{\partial \boldsymbol{y}_j^+}{\partial \lambda_0} + \frac{\partial \mathcal{N}_j}{\partial \lambda_0}\right)\mathrm{d}\lambda_0 + \sum_{q=1}^{j-1}\frac{\partial \mathcal{N}_j}{\partial t_q}\mathrm{d}t_q\end{aligned} \tag{52}$$

where

$$\frac{\partial \mathcal{N}_j}{\partial \boldsymbol{y}_{j-1}^+} = \frac{\partial \mathcal{N}_j}{\partial \boldsymbol{y}_j^-}\frac{\partial \boldsymbol{y}_j^-}{\partial \boldsymbol{y}_{j-1}^+} + \frac{\partial \mathcal{N}_j}{\partial \boldsymbol{y}_j^+}\frac{\partial \boldsymbol{y}_j^+}{\partial \boldsymbol{y}_{j-1}^+} \tag{53}$$

$$\frac{\mathrm{d}\mathcal{N}_j}{\mathrm{d}t_j} = \widehat{\mathcal{N}}_{t,j} + \check{\mathcal{N}}_{t,j}, \quad \widehat{\mathcal{N}}_{t,j} = \frac{\partial \mathcal{N}_j}{\partial \boldsymbol{y}_j^-}\dot{\boldsymbol{y}}_j^- + \frac{\partial \mathcal{N}_j}{\partial \boldsymbol{y}_j^+}\widehat{\boldsymbol{y}}_{t,j}^+, \quad \check{\mathcal{N}}_{t,j} = \frac{\partial \mathcal{N}_j}{\partial t_j} + \frac{\partial \mathcal{N}_j}{\partial \boldsymbol{y}_j^+}\check{\boldsymbol{y}}_{t,j}^+ \tag{54}$$

Then $\mathrm{d}\mathcal{N}_j/\mathrm{d}\lambda_0$ is

$$\frac{\mathrm{d}\mathcal{N}_j}{\mathrm{d}\lambda_0} = \frac{\partial \mathcal{N}_j}{\partial \boldsymbol{y}_j^-}\boldsymbol{\zeta}_j^- + \frac{\partial \mathcal{N}_j}{\partial \boldsymbol{y}_j^+}\boldsymbol{\zeta}_j^+ + \frac{\partial \mathcal{N}_j}{\partial \lambda_0} \tag{55}$$

The terms related to $\mathrm{d}\boldsymbol{x}_{d,j}^+$, $\mathrm{d}\kappa_j$ and $\mathrm{d}\alpha_j$ do not appear in flyby and rendezvous cases. Note that variables $\boldsymbol{\lambda}_{c,j}^+$ and $\boldsymbol{\lambda}_{d,j}^+$ in $\mathcal{N}_j$ should be expressed based on Eqs. (20), (29), and (31) accordingly before deriving $\partial \mathcal{N}_j/\partial \boldsymbol{x}_{d,j}^+$, $\partial \mathcal{N}_j/\partial \chi_j$, and $\partial \mathcal{N}_j/\partial \boldsymbol{\kappa}_j$.

Two equality constraints are taken as examples, i.e., $\boldsymbol{h}_j$ in Eqs. (17) and (18) that only involves continuous state component, and ϕ_j in Eq. (24) that involves both continuous and discontinuous state component. The differential of $\boldsymbol{h}_j$ is

$$\mathrm{d}\boldsymbol{h}_j = \frac{\partial \boldsymbol{h}_j}{\partial \boldsymbol{x}_{c,j}}\frac{\partial \boldsymbol{x}_{c,j}}{\partial \boldsymbol{y}_{j-1}^+}\mathrm{d}\boldsymbol{y}_{j-1}^+ + \frac{\mathrm{d}\boldsymbol{h}_j}{\mathrm{d}t_j}\mathrm{d}t_j + \frac{\partial \boldsymbol{h}_j}{\partial \boldsymbol{x}_{c,j}}\frac{\partial \boldsymbol{x}_{c,j}}{\partial \lambda_0}\mathrm{d}\lambda_0 + \sum_{q=1}^{j-1}\frac{\partial \boldsymbol{h}_j}{\partial t_q}\mathrm{d}t_q \tag{56}$$

where

$$\frac{\mathrm{d}\boldsymbol{h}_j}{\mathrm{d}t_j} = \widehat{\boldsymbol{h}}_{t,j} + \check{\boldsymbol{h}}_{t,j}, \quad \widehat{\boldsymbol{h}}_{t,j} = \boldsymbol{\nu}_j, \quad \check{\boldsymbol{h}}_{t,j} = -\boldsymbol{\nu}_{T,j} \tag{57}$$

Then $\mathrm{d}\boldsymbol{h}_j/\mathrm{d}\lambda_0$ is

$$\frac{\mathrm{d}\boldsymbol{h}_j}{\mathrm{d}\lambda_0}=\frac{\partial \boldsymbol{h}_j}{\partial \boldsymbol{x}_{c,j}}\frac{\mathrm{d}\boldsymbol{x}_{c,j}}{\mathrm{d}\lambda_0} \tag{58}$$

The values of $\partial \boldsymbol{x}_{c,j}/\partial \boldsymbol{y}_{j-1}^{+}$ and $\mathrm{d}\boldsymbol{x}_{c,j}/\mathrm{d}\lambda_0$ are extracted from $\Phi(t_j^-, t_{j-1}^+)$ and $\boldsymbol{\zeta}_j^-$, respectively.

The differential of ϕ_j is

$$\mathrm{d}\phi_j=\frac{\partial \phi_j}{\partial \boldsymbol{x}_{d,j}^-}\frac{\partial \boldsymbol{x}_{d,j}^-}{\partial \boldsymbol{y}_{j-1}^+}\mathrm{d}\boldsymbol{y}_{j-1}^+ + \frac{\partial \phi_j}{\partial \boldsymbol{x}_{d,j}^+}\mathrm{d}\boldsymbol{x}_{d,j}^+ + \frac{\mathrm{d}\phi_j}{\mathrm{d}t_j}\mathrm{d}t_j + \frac{\partial \phi_j}{\partial \boldsymbol{x}_{d,j}^-}\frac{\partial \boldsymbol{x}_{d,j}^-}{\partial \lambda_0}\mathrm{d}\lambda_0 + \sum_{q=1}^{j-1}\frac{\partial \phi_j}{\partial t_q}\mathrm{d}t_q \tag{59}$$

where

$$\frac{\mathrm{d}\phi_j}{\mathrm{d}t_j}=\widehat{\phi}_{t,j}+\breve{\phi}_{t,j},\quad \widehat{\phi}_{t,j}=\frac{\partial \phi_j}{\partial \boldsymbol{x}_{d,j}^-}\dot{\boldsymbol{x}}_{d,j}^-,\quad \breve{\phi}_{t,j}=\frac{\partial \phi_j}{\partial t_j} \tag{60}$$

Then $\mathrm{d}\phi_j/\mathrm{d}\lambda_0$ is

$$\frac{\mathrm{d}\phi_j}{\mathrm{d}\lambda_0}=\frac{\partial \phi_j}{\partial \boldsymbol{x}_{d,j}^-}\frac{\mathrm{d}\boldsymbol{x}_{d,j}^-}{\mathrm{d}\lambda_0} \tag{61}$$

In Eqs. (59-61), $\partial\phi_j/\partial \boldsymbol{x}_{d,j}^- = \left(\boldsymbol{v}_\infty^-\right)^\top/v_\infty^-$, $\partial\phi_j/\partial \boldsymbol{x}_{d,j}^+ = -\left(\boldsymbol{v}_\infty^+\right)^\top/v_\infty^+$, $\partial\phi_j/\partial t_j = -\boldsymbol{a}_{\mathrm{T},j}^\top \boldsymbol{v}_\infty^-/v_\infty^- + \boldsymbol{a}_{\mathrm{T},j}^\top \boldsymbol{v}_\infty^+/v_\infty^+$, and $\boldsymbol{a}_{\mathrm{T},j} = -\mu_j \boldsymbol{r}_{\mathrm{T},j}/\|\boldsymbol{r}_{\mathrm{T},j}\|^3$. Besides, the inequality constraint in Eq. (25) is handled as the equality constraint in Eq. (26) by using the slack variable. The differential of Eq. (26) can be carried out by referring to the differential of ϕ_j. The derivation of $\mathrm{d}\boldsymbol{y}_j^+$ in Sec. III.B and differentials of all constraints are provided as the external material*. These derivatives can be implemented with much less efforts by using MATLAB symbolic tools.

For the second step, the derivative formulae are different based on whether the decision variable is the time or not. For variables $\boldsymbol{\chi}_{j-q}$, $\boldsymbol{x}_{d,j-q}^+$, α_{j-q} or κ_{j-q}, the process to calculate the derivative of $\mathcal{N}_j$ is the same. Take $\partial\mathcal{N}_j/\partial\boldsymbol{\chi}_{j-q}$ as an example. When $q=1$, there exists

$$\frac{\partial \mathcal{N}_j}{\partial \boldsymbol{\chi}_{j-1}}=\frac{\partial \mathcal{N}_j}{\partial \boldsymbol{y}_{j-1}^+}\frac{\partial \boldsymbol{y}_{j-1}^+}{\partial \boldsymbol{\chi}_{j-1}} \tag{62}$$

The value of $\partial\mathcal{N}_j/\partial\boldsymbol{\chi}_{j-q}$ $(q>1)$ is determined by using the chain rule as

$$\frac{\partial \mathcal{N}_j}{\partial \boldsymbol{\chi}_{j-q}}=\frac{\partial \mathcal{N}_j}{\partial \boldsymbol{y}_{j-1}^+}\frac{\partial \boldsymbol{y}_{j-1}^+}{\partial \boldsymbol{y}_{j-2}^+}\cdots\frac{\partial \boldsymbol{y}_{j-q+1}^+}{\partial \boldsymbol{y}_{j-q}^+}\frac{\partial \boldsymbol{y}_{j-q}^+}{\partial \boldsymbol{\chi}_{j-q}} \tag{63}$$

If the decision variable is the interior-point time, the calculation of $\mathrm{d}\mathcal{N}_j/\mathrm{d}t_{j-1}$ is divided into two parts, i.e.,

$$\frac{\mathrm{d}\mathcal{N}_j}{\mathrm{d}t_{j-1}}=\frac{\partial \mathcal{N}_j}{\partial \boldsymbol{y}_{j-1}^+}\frac{\mathrm{d}\boldsymbol{y}_{j-1}^+}{\mathrm{d}t_{j-1}}+\frac{\partial \mathcal{N}_j}{\partial t_{j-1}} \tag{64}$$

*See http://dx.doi.org/10.13140/RG.2.2.25674.54724/1 where

$$\frac{\partial \mathcal{N}_j}{\partial t_{j-1}} = -\widehat{\mathcal{N}}_{t,j} \tag{65}$$

The term $\overset{\smile}{\mathcal{N}}_{t,j}$ is not involved in Eq. (65) since t_j is assumed unaltered at derivation.

Applying the chain rule, $\mathrm{d}\mathcal{N}_j/\mathrm{d}t_{j-q}$ ($q \geqslant 2$) can be computed as

$$\frac{\mathrm{d}\mathcal{N}_j}{\mathrm{d}t_{j-q}} = \frac{\partial \mathcal{N}_j}{\partial \mathbf{y}^+_{j-1}} \frac{\partial \mathbf{y}^+_{j-1}}{\partial \mathbf{y}^+_{j-2}} \cdots \frac{\partial \mathbf{y}^+_{j-q+1}}{\partial \mathbf{y}^+_{j-q}} \frac{\mathrm{d}\mathbf{y}^+_{j-q}}{\mathrm{d}t_{j-q}} + \frac{\partial \mathcal{N}_j}{\partial t_{j-q}} \tag{66}$$

where

$$\frac{\partial \mathcal{N}_j}{\partial t_{j-q}} = \begin{cases} -\dfrac{\partial \mathcal{N}_j}{\partial \mathbf{y}^+_{j-1}} \widehat{\mathbf{y}}^+_{t,j-1} & q = 2 \\ -\dfrac{\partial \mathcal{N}_j}{\partial \mathbf{y}^+_{j-1}} \dfrac{\partial \mathbf{y}^+_{j-1}}{\partial \mathbf{y}^+_{j-2}} \cdots \dfrac{\partial \mathbf{y}^+_{j-q+2}}{\partial \mathbf{y}^+_{j-q+1}} \widehat{\mathbf{y}}^+_{t,j-q+1} & q \geqslant 3 \end{cases} \tag{67}$$

In [17, 18], only the first term in Eq. (64) is considered. However, the second term is also necessary to produce accurate gradients in our applications (See Sec. IV.A). Eqs. (63), (64) and (66) can be used to compute derivatives of $\mathcal{N}_j$. However, the computational burden would be high if every term is computed from scratch at t_j, thus it is necessary to recursively calculate them. First, the matrix B_{j-1} is defined as

$$B_{j-1} = \frac{\partial \mathcal{N}_j}{\partial \mathbf{y}^+_{j-1}} \tag{68}$$

Next, B_l, $l = j-q, \cdots, j-2$ is computed as

$$B_l = B_{l+1} \frac{\partial \mathbf{y}^+_{l+1}}{\partial \mathbf{y}^+_l} \tag{69}$$

then

$$\frac{\partial \mathcal{N}_j}{\partial \boldsymbol{\chi}_{j-q}} = B_{j-q} \frac{\partial \mathbf{y}^+_{j-q}}{\partial \boldsymbol{\chi}_{j-q}}, \quad q \geqslant 1 \tag{70}$$

and

$$\frac{\mathrm{d}\mathcal{N}_j}{\mathrm{d}t_{j-q}} = B_{j-q} \frac{\mathrm{d}\mathbf{y}^+_{j-q}}{\mathrm{d}t_{j-q}} - B_{j-q+1} \widehat{\mathbf{y}}^+_{t,j-q+1}, \quad q \geqslant 2 \tag{71}$$

The algorithm to recursively calculate derivatives of $\mathcal{N}_j$ is shown in Algorithm 1. Note in Algorithm 1 that the term related to $\mathrm{d}\lambda_0$ in the differential such as Eq. (46) is unnecessary to compute but $\boldsymbol{\zeta}^+_j$ such as Eq. (50) is required to compute.

Algorithm 1 Calculate $\mathcal{N}_j$ and its analytic gradients.

for $k = 0 : w$ **do**{Loop each phase}
  Integrate Eq. (36) from t_k^+ to t_{k+1}^- with z_k^+.
  Extract $\Phi(t_{k+1}^+, t_k^-)$, $\boldsymbol{y}_{k+1}^-$, and $\boldsymbol{\zeta}_{k+1}^-$ from z_{k+1}^-.
  if $k \leqslant w-1$ **then** {Interior-point time is t_{k+1}.}
    $j = k+1$.
    if $\mathcal{N}_j$ is a flyby or rendezvous constraint **then**
      Compute $\boldsymbol{\lambda}_{c,j}^+$ from Eq. (20).
      Compute derivatives of $\boldsymbol{y}_j^+$ in Eqs. (43)-(45).
    else
      Compute $\boldsymbol{\lambda}_{c,j}^+$ from Eq. (29) and $\boldsymbol{\lambda}_{d,j}^+$ from Eq. (31).
      Compute derivatives of $\boldsymbol{y}_j^+$ in Eqs. (47)-(50).
    end if
    Formulate z_j^+ and compute $\mathcal{N}_j$.
    Compute derivatives of $\mathcal{N}_j$ in Eq. (52)-(54).
    Compute $\mathrm{d}\mathcal{N}_j/\mathrm{d}\lambda_0$ in Eq. (55).
    Compute B_{j-1} in Eq. (68).
    for $l = j-1 : -1 : 1$ **do**
      if $l+1 = j$ **then**
        Compute $\mathrm{d}\mathcal{N}_j/\mathrm{d}t_l$ in Eq. (64).
      else
        Compute $\mathrm{d}\mathcal{N}_j/\mathrm{d}t_l$ in Eq. (71).
      end if
      Compute $\partial\mathcal{N}_j/\partial\boldsymbol{\chi}_l$ in Eq. (70).
      Compute $\partial\mathcal{N}_j/\partial\boldsymbol{x}_{d,l}^+$, $\partial\mathcal{N}_j/\partial\alpha_l$, and $\partial\mathcal{N}_j/\partial\kappa_l$ if required.
      B_{l-1} is updated using Eq. (69).
    end for
    Extract $\partial\mathcal{N}_j/\partial\boldsymbol{\lambda}_i$ from B_0.
  end if
end for

IV. Simulations

Two simulation examples of interplanetary transfers are presented. All simulations are performed under an Intel Core i7-9750H, CPU@2.6 GHz, Windows 10 system with MATLAB R2019a. The code for integrating Eq. (36) is converted to MEX (MATLAB Executable) file to speed up simulations. Table 1 provides the physical constants used in all examples. MATLAB function `fsolve` is employed to solve the shooting problem, with the maximal iteration number as 70. The initial increment of ε is $\Delta\varepsilon = 0.05$. When the solution for current ε succeeds, a slightly larger $\Delta\varepsilon$ is awarded, as $\Delta\varepsilon \leftarrow 1.05 \times \Delta\varepsilon$, otherwise half of $\Delta\varepsilon$ is used, as $\Delta\varepsilon \leftarrow 0.5 \times \Delta\varepsilon$. The guess of unknowns for the ith step ($i \geqslant 0$) of the continuation process is denoted $\boldsymbol{p}_{i,guess}$, and the optimal solution for the ith step as $\boldsymbol{p}_i$. For $i = 1$, the guess solution is set as $\boldsymbol{p}_{1,guess} = \boldsymbol{p}_0$ with $\boldsymbol{p}_0$ as the energy-optimal solution. For $i \geqslant 2$, the guess solution is generated by using the linear interpolation, as

$$\boldsymbol{p}_{i,guess} = \frac{\boldsymbol{p}_{i-1} - \boldsymbol{p}_{i-2}}{\varepsilon_{i-1} - \varepsilon_{i-2}} \left(\varepsilon_i - \varepsilon_{i-1}\right) + \boldsymbol{p}_{i-1} \tag{72}$$

In addition, the position and velocity of planets and asteroids are calculated based on [25] and using orbital elements from Minor Planet Center [†], respectively.

Table 1 Gravitational parameters and scaling units.

Physical constant	Value
Sun mass parameter, μ_s	1.327124×10^{11} km^3/s^2
Gravitational field, g_0	9.80665 m/s^2
Astronomical unit, AU	1.495979×10^{8} km
Time unit, TU	5.022643×10^{6} s
Velocity unit, VU	29.784692 km/s

A. Earth-Jupiter Transfer via Mars Gravity Assist

The example of fuel-optimal Earth-Mars-Jupiter (EMJ) transfer with Mars gravity assist from [9] is reproduced, with the transfer duration as 2201 days. The spacecraft parameters, Mars parameters and boundary conditions are given in Table 2, where the initial and terminal heliocentric position and velocity of the spacecraft are set to coincide with those of the Earth and Jupiter, respectively.

The unknowns are $[\lambda_0, \boldsymbol{\lambda}_i, \boldsymbol{\chi}_1, \boldsymbol{x}^+_{d,1}, \alpha_1, \kappa_1, t_1] \in \mathbb{R}^{18}$, with $\boldsymbol{\lambda}_i \in \mathbb{R}^7$, $\boldsymbol{\chi}_1 \in \mathbb{R}^4$ and $\boldsymbol{x}^+_{d,1} \in \mathbb{R}^3$. Both energy- and fuel-optimal solutions are summarized in Table 3, where the fuel-optimal final mass of the spacecraft is 16027.3 kg. The fuel-optimal trajectory is shown in Fig. 2, involving four thrust segments and three coast segments. The corresponding fuel-optimal variations of u, S, m are shown in Fig. 3, where red solid line and blue dashed line coincide with Fig. 2, and blue dotted line labels the discontinuity. The boundary conditions are slightly different from [9], but their impact on the fuel-optimal solution is negligible. This can be seen from the facts that the bang-bang control profile coincides with each other, and the difference on the final mass (16022 kg in [9]) is admissible (0.13% of the fuel consumption). Also, the difference of final mass between our result and the result from [26] (16026 kg) is very small.

Regarding the computational time, the continuation using the presented method takes about 20 s, while the continuation with the FD method inherently embedded in MATLAB takes about 40 s. Note that only Eq. (13), instead of Eq. (36), is used for dynamical integration in the FD method. The computational efficiency of our method is superior than the FD method by a factor of 2. The computational time for both analytic gradients and the FD method is much less than the work in [9] (about 3 mins), which is executed using the solution of the ith step as the guess solution of the $(i+1)$th step under Microsoft Visual C++ 6.0 with 4th-order Runge–Kutta integrator.

To verify that the derivatives with respect to the gravity-assist time require the second term in Eq. (64), the comparison between the FD method and analytic gradients on the derivative of terminal conditions in Eq. (4) with

[†] See https://minorplanetcenter.net/

respect to the gravity-assist time is executed. The central FD method is used, as [13]

$$f'(x) = \frac{-f(x+2\eta) + 8f(x+\eta) - 8f(x-\eta) + f(x-2\eta)}{12\eta} \tag{73}$$

where $\eta = 1 \times 10^{-6}$ is the step size. Denote the derivatives obtained by Eq. (73) and analytic gradients as $J_{\text{FD}} \in \mathbb{R}^6$ and $J_{\text{AG}} \in \mathbb{R}^6$. Since there is only one interior-point constraint, and the control of the energy-optimal solution is continuous except at the interior-point time, the gradients calculated based on the energy-optimal solution from the FD method can be used as the reference. The relative error $\max_{i=1,2,\cdots,6} |(J_{\text{FD}}(i) - J_{\text{AG}}(i))/J_{\text{FD}}(i)|$ is calculated to represent the gradient accuracy. The relative error is about 3.3×10^{-5} when Eq. (64) is applied, while about 4.3×10^{-3} is obtained when only the first term of Eq. (64) is used, indicating that the second term of Eq. (64) is indeed required for the accuracy of analytic gradients.

Table 2 Parameters for EMJ transfer.

Physical constant	Value
I_{sp}, s	6000
$T_{\max}$, N	2.26
Initial mass, kg	20000.0
Mars mass parameter, km^3/s^2	42828.3
Mars $r_{\min}$, km	3889.9
Mars radius, km	3389.9
Initial time	16-Nov-2021, 00:00:00
Flight time, days	2201.0
Initial position, AU	[0.587638, 0.795476, -3.953062×10^{-5}]
Initial velocity, VU	[-0.820718, 0.590502, -2.934460×10^{-5}]
terminal position, AU	[-5.205108, 1.491385, 0.110274]
terminal velocity, VU	[-0.126219, -0.401428, 4.494423×10^{-3}]

B. Earth-Earth Transfer via Venus gravity assist, asteroids flyby and Rendezvous

The fuel-optimal Earth-Venus-2014 YD-2000 SG344-Earth (EVYSE) transfer, involving Venus gravity assist, 2014 YD flyby and 2000 SG344 rendezvous, is solved. These asteroids are selected from the preliminary result of asteroid screening for the Miniaturised Asteroid Remote Geophysical Observer (M-ARGO) in [27]. Orbital elements of the asteroids are listed in Table 4. Spacecraft parameters and boundary conditions are shown in Table 5, where the initial and terminal heliocentric position and velocity of the spacecraft are set to coincide with those of the Earth. The unknowns to solve are $[\lambda_0, \boldsymbol{\lambda}_i, \boldsymbol{\chi}_1, \boldsymbol{x}^+_{d.1}, \alpha_1, \kappa_1, t_1, \boldsymbol{\chi}_2, t_2, \boldsymbol{\chi}_3, t_3] \in \mathbb{R}^{29}$, with $\boldsymbol{\chi}_1 \in \mathbb{R}^4$, $\boldsymbol{\chi}_2 \in \mathbb{R}^3$ and $\boldsymbol{\chi}_3 \in \mathbb{R}^6$. Energy- and fuel-optimal solutions are given in Table 6. The fuel-optimal trajectory is shown in Fig. 4, consisting of 7 thrust arcs and 6 coast arcs. The corresponding u, S and m are illustrated in Fig. 5. The variations of costates are shown in

Table 3 Energy- and fuel-optimal solutions for the EMJ transfer.

Terms	Energy-optimal solution	Fuel-optimal solution
λ_0	0.615841	0.819085
$\boldsymbol{\lambda}_{ri}$	[-0.278574, -0.459643, -0.053818]	[-0.211713, -0.293487, -0.031748]
$\boldsymbol{\lambda}_{vi}$	[0.362598, -0.334005, -0.055783]	[0.279598, -0.208178, -0.085726]
$\boldsymbol{\lambda}_{mi}$	0.176741	0.177985
$\boldsymbol{\chi}_1$	[-0.007492, -0.103902, 0.062598, -0.191078]	[0.026271, -0.058226, 0.077165, -0.161649]
$\boldsymbol{x}_{d,1}^+$, VU	[0.912146, 0.285078, -0.004974]	[0.820778, 0.514477, -0.003464]
κ_1	0.017362	0.020703
α_1	0	0
GA date t_1	19 Feb 2024	19 Mar 2024
GA v_∞, km/s	3.189	3.602
GA altitude, km	500	500
Final mass, kg	15742.7	16027.3

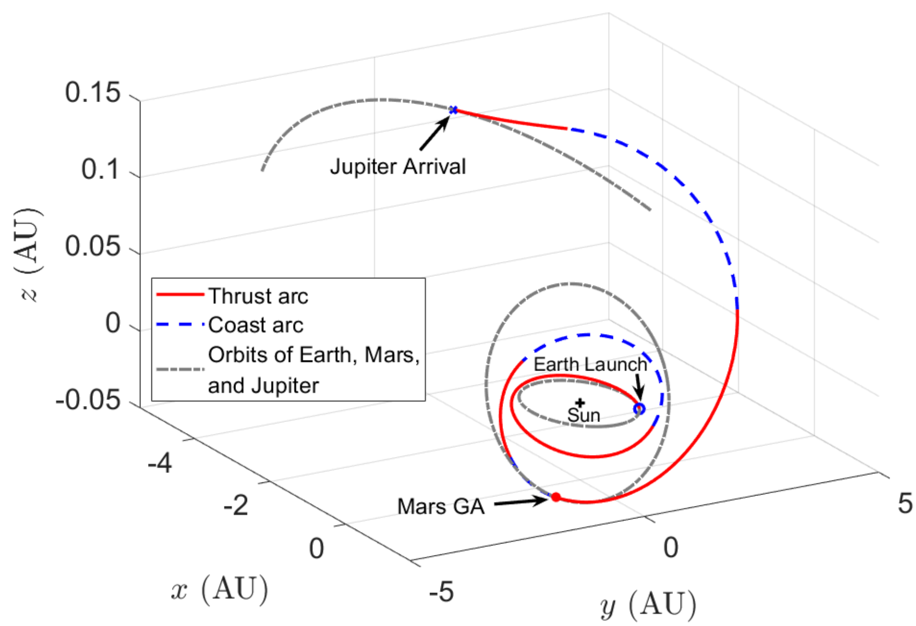

Fig. 2 Fuel-optimal trajectory for the EMJ trajectory.

Fig. 6, where the costate discontinuities across the interior-point time are illustrated.

The computational time of energy-to-fuel-optimal continuation for the presented method is about 14.6 mins, which takes longer time than the EMJ trajectory, because the increased sensitivity requires smaller $\Delta\varepsilon$ during the continuation. When the FD method is employed, the continuation fails and terminates at $\varepsilon \approx 0.045$ since $\Delta\varepsilon$ is smaller than the threshold ($\Delta\varepsilon \leqslant 1.0 \times 10^{-6}$) after about 3.2 hours of computation. A comparison with the solution from the General Purpose Optimal Control Software (GPOPS) [28] is performed, see Table 6 and Fig. 7. It is clear that the GPOPS

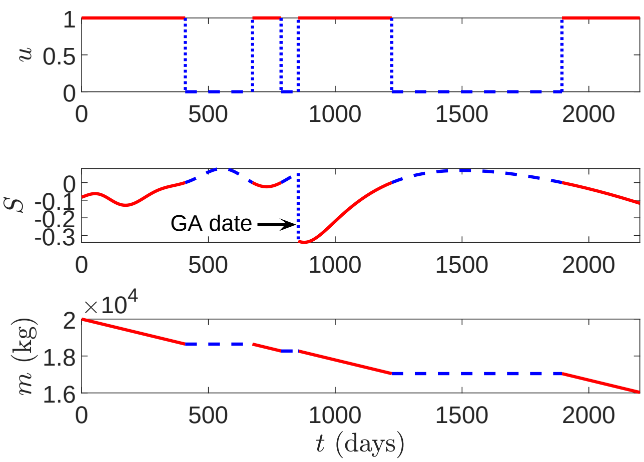

Fig. 3 Fuel-optimal variations of u, S, and m for the EMJ trajectory.

solution coincides with the solution obtained by using the presented method. Compared to the GPOPS solution, our method enables to obtain the fuel-optimal bang-bang solution featuring with accurate switching time. On the other hand, our tests indicate that it is difficult to find a solution that satisfies the optimality tolerance lower than 1.0×10^{-5} by using GPOPS. Also, since much fewer unknowns are required to solve for the indirect method, evolutionary algorithms can be applied to broadly searching initial guesses of the energy-optimal problem with a small number of unknowns [9]. Evolutionary algorithms do not require accurate gradients in general, and the outcome is a guess solution that does not accurately satisfy the necessary conditions of optimality. Once a guess solution is found, the analytic gradients developed in this work can be used to further determine the accurate energy- and fuel-optimal solutions. We believe that a hybrid algorithm that combines an evolutionary algorithm and analytic gradients would improve effectiveness and efficiency on obtaining a convergent solution. However, the proof of this conjecture is unnecessary for this Note.

Table 4 Orbital elements of 2014 YD and 2000 SG344.

Terms	2014 YD	2000 SG344
Semimajor axis (AU)	1.072142	0.9774614
Eccentricity	0.0866205	0.0669332
Inclination (deg)	1.73575	0.11213
Longitude of ascending node (deg)	117.64009	191.95995
Argument of perihelion (deg)	34.11615	275.30264
Mean anomaly at epoch (deg)	278.1406	347.71212
Epoch	27 May 2019	27 May 2019

Table 5 Parameters for the EVYSE trajectory.

Physical constant	Value
I_{sp}, s	2300
$T_{\max}$, N	0.75
Initial mass, kg	1300
Venus mass parameter, km^3/s^2	324858.592
Venus $r_{\min}$, km	21051.8
Venus radius, km	6051.8
Launch date	13 Apr 2015, 00:00:00
Arrival date	01 Nov 2017, 00:00:00
Initial position, AU	[-0.925875, -0.384412, 1.337409×10^{-5}]
Initial velocity, VU	[0.367225, -0.927443, 3.226668×10^{-5}]
terminal position, AU	[0.776680, 0.618052, -2.507007×10^{-5}]
terminal velocity, VU	[-0.639034, 0.778835, -3.159191×10^{-5}]

Table 6 Energy-optimal, fuel-optimal and GPOPS solutions for the EVYSE transfer.

Terms	Energy-optimal solution	Fuel-optimal solution	GPOPS solution
λ_0	0.614541	0.532128	-
λ_{ri}	[-0.128983, -0.002532, -0.116029]	[0.101367, 0.103705, -0.087083]	-
λ_{vi}	[0.207334, -0.270715, -0.007851]	[0.179221, -0.045626, 0.006821]	-
λ_{mi}	0.467548	0.446129	-
χ_1	[0.265046, 0.197794, 0.162365, -0.070416]	[0.364608, 0.127974, 0.137367, -0.029487]	-
κ_1	0.008614	0.011356	-
α_1	0	0	0
$\boldsymbol{x}_{d,1}^{+}$, VU	[-0.523540, 1.223757, 0.011536]	[-0.193133, 1.321951, 0.009115]	[-0.194831, 1.321486, 0.008853]
GA date t_1	23 Sept 2015	13 Sept 2015	13 Sept 2015
GA v_∞, km/s	4.8075	4.9393	4.9344
GA altitude, km	15000	15000	15000
χ_2	[0.048014, -0.032200, -0.014900]	[0.046725, -0.046363, -0.014239]	-
Flyby date t_2	05 May 2016	21 Apr 2016	21 Apr 2016
χ_3	[-0.110824, -0.180728, 0.019802	[-0.278104, -0.213831, 0.040000	-
	-0.233212, 0.114268, 0.013552]	-0.227530, 0.323050, 0.020738]	-
Rendezvous date t_3	26 Nov 2016	01 Nov 2016	02 Nov 2016
Final mass, kg	193.02	339.82	340.14

Conclusions

Gradient accuracy is significant when solving low-thrust trajectories with flybys, rendezvous, and gravity assists, due to the discontinuities produced by the bang-bang control and the time-dependent interior-point constraints. This work investigates the benefits of analytic gradients on solving this problem. The formulation of the normalized low-thrust optimization is employed, since it allows searching multipliers and initial costates by restricting them on a unit hypersphere. Gradients are strictly analyzed and their analytical expressions are obtained, although gradients are discontinuous at epochs of the interior point and bang-bang controls. The recursive formulae of the chain rule

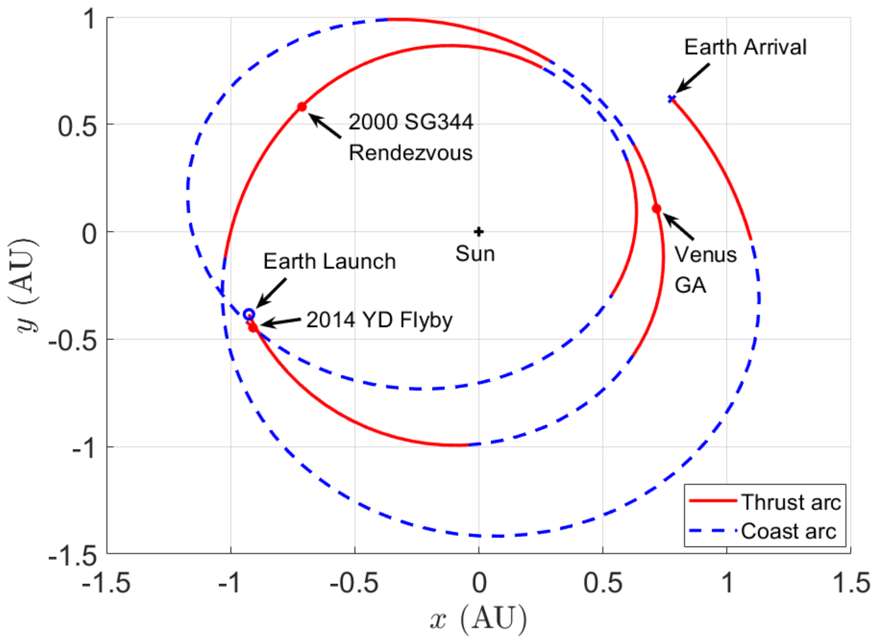

Fig. 4 Fuel-optimal trajectory for the EVYSE trajectory.

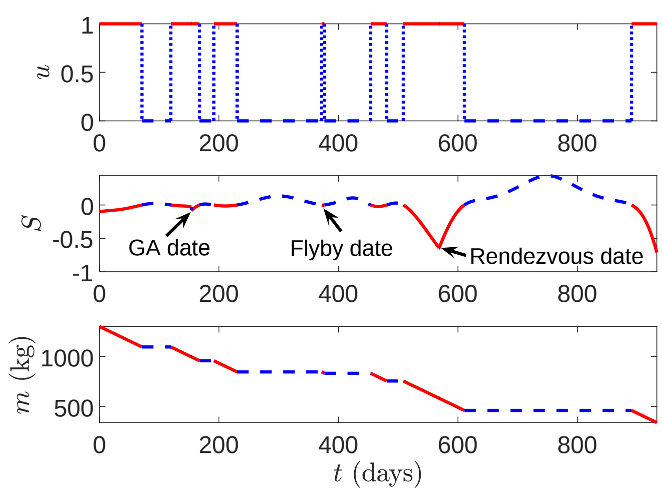

Fig. 5 Fuel-optimal variations of u, S, and m for the EVYSE trajectory.

to calculate gradients are developed, which can be commonly applied to other problems that involve interior-point constraints. The outcome is a computational framework that incorporates analytic gradients, energy-to-fuel-optimal continuation, and the integration flowchart embedded with the switching detection, which has the advantage of offering the desired fuel-optimal bang-bang solutions and their gradients.

Two numerical examples of interplanetary transfers are simulated, and the obtained solutions are verified against either the existing solution in literature or the solution from the direct method. The comparison with the finite difference method is executed, verifying the formulae developed in this work that calculates gradients with respect to the

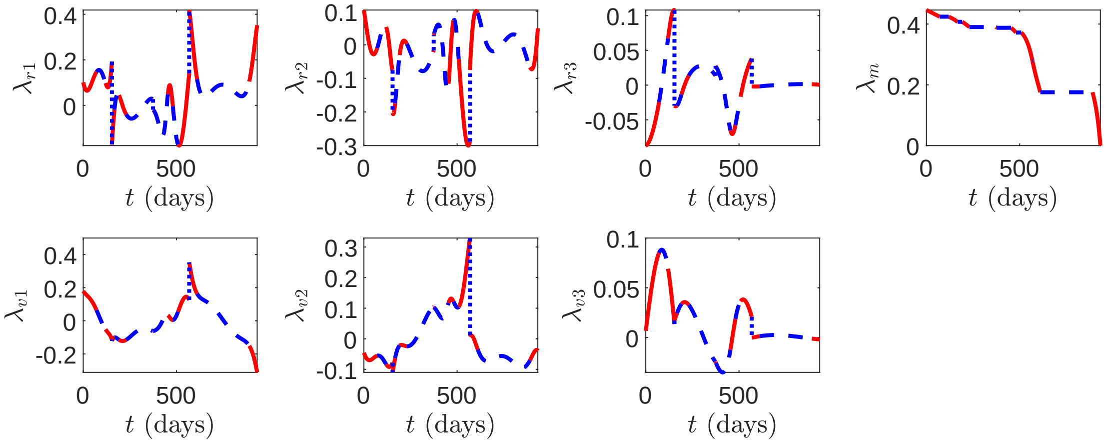

Fig. 6 Fuel-optimal variations of costates for the EVYSE trajectory.

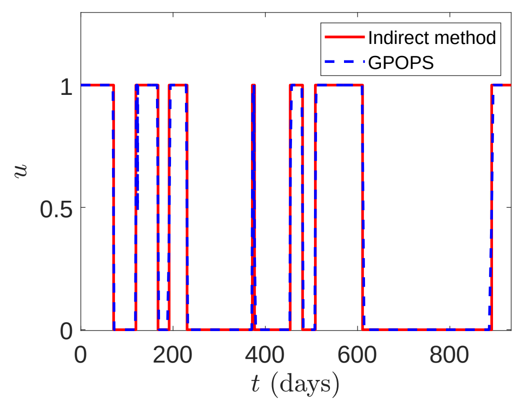

Fig. 7 Comparison of fuel-optimal thrust throttle profile to the GPOPS solution.

interior-point time, and indicating that the presented method enables to enhance effectively both the solver execution speed and its convergence performance compared to the finite difference method.

Acknowledgment

Y. W. thanks the support from China Scholarship Council (No. 201706290024) and International Postdoctoral Exchange Fellowship Program of China (No. YJ20220105). X. Y. H. thanks the support from National Natural Science Foundation of China (No. 12233003).

References

[1] Vavrina, M., and Howell, K., "Multiobjective Optimization of Low-Thrust Trajectories Using a Genetic Algorithm Hybrid," *AAS/AIAA Space Flight Mechanics Metting*, Savannah, Georgia, 2009. AAS 09-151.

[2] Brown, C., *Spacecraft Mission Design*, 2$^{\text{nd}}$ ed., American Institute of Aeronautics and Astronautics, Reston, 1998. p. 120.

[3] McConaghy, T., Debban, T., Petropoulos, A., and Longuski, J., "Design and Optimization of Low-Thrust Trajectories with Gravity Assists," *Journal of Spacecraft & Rockets*, Vol. 40, No. 3, 2003, pp. 380–387. doi:10.2514/2.3973.

[4] Olympio, J., "Optimal Control Problem for Low-Thrust Multiple Asteroid Tour Missions," *Journal of guidance, control, and dynamics*, Vol. 34, No. 6, 2011, pp. 1709–1720. doi:10.2514/1.53339.

[5] Morante, D., Sanjurjo Rivo, M., and Soler, M., "A Survey on Low-Thrust Trajectory Optimization Approaches," *Aerospace*, Vol. 8, No. 3, 2021, p. 88. doi:10.3390/aerospace8030088.

[6] Petropoulos, A., and Longuski, J., "Shape-Based Algorithm for the Automated Design of Low-Thrust, Gravity Assist Trajectories," *Journal of Spacecraft and Rockets*, Vol. 41, No. 5, 2004, pp. 787–796. doi:10.2514/1.13095.

[7] Morante, D., Sanjurjo Rivo, M., and Soler, M., "Multi-Objective Low-Thrust Interplanetary Trajectory Optimization Based on Generalized Logarithmic Spirals," *Journal of Guidance, Control, and Dynamics*, Vol. 42, No. 3, 2019, pp. 476–490. doi:10.2514/1.G003702.

[8] Ellison, D., Conway, B., Englander, J., and Ozimek, M., "Analytic Gradient Computation for Bounded-Impulse Trajectory Models Using Two-Sided Shooting," *Journal of Guidance, Control, and Dynamics*, Vol. 41, No. 7, 2018, pp. 1449–1462. doi:10.2514/1.G003077.

[9] Jiang, F., Baoyin, H., and Li, J., "Practical Techniques for Low-Thrust Trajectory Optimization with Homotopic Approach," *Journal of Guidance, Control, and Dynamics*, Vol. 35, No. 1, 2012, pp. 245–258. doi:10.2514/1.52476.

[10] Jiang, F., and Tang, G., "Systematic Low-Thrust Trajectory Optimization for a Multi-Rendezvous Mission Using Adjoint Scaling," *Astrophysics and Space Science*, Vol. 361, No. 4, 2016, p. 117. doi:10.1007/s10509-016-2704-5.

[11] Chi, Z., Jiang, F., and Tang, G., "Optimization of Variable-Specific-Impulse Gravity-Assist Trajectories via Optimality-Preserving Transformation," *Aerospace Science and Technology*, Vol. 101, 2020, p. 105828. doi:10.1016/j.ast.2020.105828.

[12] Arya, V., Taheri, E., and Junkins, J., "Low-Thrust Gravity-Assist Trajectory Design Using Optimal Multimode Propulsion Models," *Journal of Guidance, Control, and Dynamics*, Vol. 44, No. 7, 2021, pp. 1280–1294. doi:10.2514/1.G005750.

[13] Fornberg, B., "Generation of Finite Difference Formulas on Arbitrarily Spaced Grids," *Mathematics of computation*, Vol. 51, No. 184, 1988, pp. 699–706. doi:10.1090/S0025-5718-1988-0935077-0.

[14] Squire, W., and Trapp, G., "Using Complex Variables to Estimate Derivatives of Real Functions," *SIAM review*, Vol. 40, No. 1, 1998, pp. 110–112. doi:10.1137/S003614459631241X.

[15] Russell, R., "Primer Vector Theory Applied to Global Low-Thrust Trade Studies," *Journal of Guidance, Control, and Dynamics*, Vol. 30, No. 2, 2007, pp. 460–472. doi:10.2514/1.22984.

[16] Ocampo, C., and Munoz, J.-P., "Variational Equations for a Generalized Spacecraft Trajectory Model," *Journal of Guidance, Control, and Dynamics*, Vol. 33, No. 5, 2010, pp. 1615–1622. doi:10.2514/1.46953.

[17] Zimmer, S., and Ocampo, C., "Analytical Gradients for Gravity Assist Trajectories Using Constant Specific Impulse Engines," *Journal of Guidance, Control, and Dynamics*, Vol. 28, No. 4, 2005, pp. 753–760. doi:10.2514/1.9917.

[18] Zimmer, S., and Ocampo, C., "Use of Analytical Gradients to Calculate Optimal Gravity-Assist Trajectories," *Journal of Guidance, Control, and Dynamics*, Vol. 28, No. 2, 2005, pp. 324–332. doi:10.2514/1.4825.

[19] Zhang, C., Topputo, F., Bernelli-Zazzera, F., and Zhao, Y., "Low-Thrust Minimum-Fuel Optimization in the Circular Restricted Three-Body Problem," *Journal of Guidance, Control, and Dynamics*, Vol. 38, No. 8, 2015, pp. 1501–1510. doi:10.2514/1.G001080.

[20] Yang, H., Li, J., and Baoyin, H., "Low-Cost Transfer between Asteroids with Distant Orbits Using Multiple Gravity Assists," *Advances in Space Research*, Vol. 56, No. 5, 2015, pp. 837–847. doi:10.1016/j.asr.2015.05.013.

[21] Bertrand, R., and Epenoy, R., "New Smoothing Techniques for Solving Bang–Bang Optimal Control Problems–Numerical Results and Statistical Interpretation," *Optimal Control Applications and Methods*, Vol. 23, No. 4, 2002, pp. 171–197. doi:10.1002/oca.709.

[22] Bryson, A., and Ho, Y.-C., *Applied Optimal Control: Optimization, Estimation and Control*, Taylor and Francis Group, New York, 1975. Chapters 2-3.

[23] Hull, D., *Optimal Control Theory for Applications*, Springer-Verlag, New York, 2013. Chapter 4.

[24] Wang, Y., and Topputo, F., "Indirect Optimization of Fuel-Optimal Many-Revolution Low-Thrust Transfers with Eclipses," *IEEE Transactions on Aerospace and Electronic Systems*, Vol. 59, No. 1, 2023, pp. 39–51. doi:10.1109/TAES.2022.3189330.

[25] Standish, M., and Williams, J., *Orbital Ephemerides of the Sun, Moon, and Planets*, University Science Books, 1992. Chapter 8.

[26] Yam, C. H., McConaghy, T., Chen, J., and Longuski, J., "Preliminary Design of Nuclear Electric Propulsion Missions to the Outer Planets," *AIAA/AAS Astrodynamics Specialist Conference and Exhibit*, Providence, Rhode Island, 2004. doi: 10.2514/6.2004-5393, AIAA 2004-5393.

[27] Topputo, F., Wang, Y., Giordano, C., Franzese, V., Goldberg, H., Perez-Lissi, F., and Walker, R., "Envelop of Reachable Asteroids by M-ARGO CubeSat," *Advances in Space Research*, Vol. 67, No. 12, 2021, pp. 4193–4221. doi:10.1016/j.asr.2021.02.031.

[28] Rao, A., Benson, D., Darby, C., Patterson, M., Francolin, C., Sanders, I., and Huntington, G., "Algorithm 902: GPOPS, A MATLAB Software for Solving Multiple-Phase Optimal Control Problems Using the Gauss Pseudospectral Method," *ACM Transactions on Mathematical Software*, Vol. 37, 2010, pp. 1–39. doi:10.1145/1731022.1731032.